

## Accepted Article

**Title:** Polymorphism of Erbium Oxyfluoride: Selective Synthesis, Crystal Structure and Phase-Dependent Upconversion Luminescence

**Authors:** Ting Wen, Ruixian Ding, Yannan Zhou, Yubing Si, Baocheng Yang, and Yonggang Wang

This manuscript has been accepted after peer review and appears as an Accepted Article online prior to editing, proofing, and formal publication of the final Version of Record (VoR). This work is currently citable by using the Digital Object Identifier (DOI) given below. The VoR will be published online in Early View as soon as possible and may be different to this Accepted Article as a result of editing. Readers should obtain the VoR from the journal website shown below when it is published to ensure accuracy of information. The authors are responsible for the content of this Accepted Article.

**To be cited as:** *Eur. J. Inorg. Chem.* 10.1002/ejic.201700658

**Link to VoR:** <http://dx.doi.org/10.1002/ejic.201700658>

# Polymorphism of Erbium Oxyfluoride: Selective Synthesis, Crystal Structure and Phase-Dependent Upconversion Luminescence

Ting Wen,<sup>\*,[a,b]</sup> Ruixian Ding,<sup>[a]</sup> Yannan Zhou,<sup>[a,b]</sup> Yubing Si,<sup>[a,b]</sup> Baocheng Yang<sup>\*,[a,b]</sup> and Yonggang Wang<sup>\*,[c]</sup>

**Abstract:** Phase-selective synthesis and structure switching behavior of a functional material are essential to enable comparative studies on the structure-property relationship. Here, we report a controllable fluorination route to phase-pure erbium oxyfluorides with orthorhombic (O-ErOF) and rhombohedral (R-ErOF) structures. This facile method adopts polytetrafluoroethylene (PTFE) as the fluidizer and the phase selectivity can be easily achieved at specific fluorination temperatures. The phase evolution and detailed crystal structures of erbium oxyfluoride were characterized by powder X-ray diffraction at various sintering temperatures and Rietveld refinements, respectively. An irreversible phase transition from O-ErOF to R-ErOF was observed under heating around 600 °C. The upconversion (UC) luminescence properties of R-ErOF and O-ErOF were studied comparatively by means of photoluminescence, *P-I* and UC decay curves. Despite their similar component and crystal structure, R-ErOF exhibits stronger (more than 20 times) red UC emission than O-ErOF. The anomalous UC behavior of the two polymorphisms of ErOF was associated with the energy transfer processes dependent on their crystal structure features.

## Introduction

Trivalent rare-earth ions (RE<sup>3+</sup>)-doped upconversion (UC) luminescent materials that can convert near-infrared (NIR) photons into visible emissions exhibits applied potentialities in the fields such as colour displays, photovoltaics, solid-state lasers and biological imaging owing to their low autofluorescence background, sharp emission bandwidths and superior photostabilities.<sup>1</sup> Since UC luminescence is a multi-photon processes among the neighbouring RE<sup>3+</sup> dopants (sensitizer and activator) spatially distributed in a host matrix, the host structure plays a significant role in

deciding the site symmetry, the strength of crystal-fields and thus the f-f transition probabilities.<sup>2</sup> It is also known that the geometric relationship of the RE cations in the host matrices affect the interplays between adjacent RE centers directly.<sup>3</sup> Therefore crystal structure variation of the host materials is considered as an effective way to regulate the optical properties of RE-based UC phosphors, including the emission efficiency and the emitting band selectivity. Take the NaYF<sub>4</sub>:Yb/Er UC phosphor as an example, the green emissions (525 nm, <sup>2</sup>H<sub>11/2</sub>→<sup>4</sup>I<sub>15/2</sub>; 542 nm, <sup>4</sup>S<sub>3/2</sub>→<sup>4</sup>I<sub>15/2</sub>) in hexagonal NaYF<sub>4</sub> host materials are about an order of magnitude more intense than those in their cubic counterparts.<sup>4</sup> On the other hand, UC emission G/R (green/red) ratios of the hexagonal and cubic phases presents an opposite tendency.<sup>5</sup> Crystallographic phase control of NaYF<sub>4</sub>:Yb/Er nanoparticles by Gd<sup>3+</sup> ions doping lead to tunable UC emission colours (orange to green) and the UC emission G/R ratio of the hexagonal phase is over twice higher than that of the cubic-hexagonal-mixed phase.<sup>6</sup>

Lanthanide oxyfluorides are considered to be attractive candidates for UC host materials owing to their combination of both merits of fluorides and oxides counterparts, such as low phonon energy, excellent mechanical strength, and good chemical and thermal stability. Thus, RE<sup>3+</sup> doped lanthanide oxyfluorides have been frequently reported exhibiting intense and multifarious UC photoluminescence properties.<sup>7</sup> Significantly, lanthanide oxyfluorides crystallize in several distinct polymorphisms, such as the cubic fluorite structure, the tetragonal PbFCl-type, the rhombohedral SmSI-type, and the orthorhombic Vernier-type with an incommensurate structure.<sup>8</sup> Almost all of these structures originate from fluorite structure which has been proved to be the best UC host lattice (such as CaF<sub>2</sub> and NaREF<sub>4</sub>).<sup>9</sup> The transmutation of them depends on the stoichiometric ratio between O<sup>2-</sup> and F<sup>-</sup> ions and the arrangement ordering of anions in the lattice.<sup>10</sup> So, it is not surprising to see a given lanthanide oxyfluoride adopting several different structures through similar synthetic routes and also the reversible or irreversible transition between these allotropes. For example, lanthanum oxyfluoride (LaOF) crystallized in cubic, tetragonal and trigonal structures through thermal decomposition of the same precursor under different conditions.<sup>11</sup> These structure-selective or phase-switching systems are perfect candidates for comparative studies on the structure-property relationship of UC luminescence materials, and the exploration of new systems is of timely urgency.

In our previous works, we have studied the crystal structures and UC properties of a series of Vernier-phase lanthanide oxyfluorides as the host for RE<sup>3+</sup> doping, such as Y<sub>6</sub>O<sub>5</sub>F<sub>8</sub>, Lu<sub>5</sub>O<sub>4</sub>F<sub>7</sub> and Yb<sub>5</sub>O<sub>4</sub>F<sub>7</sub>.<sup>12</sup> Despite the similarity of their chemical formula and structure prototypes, they do exhibit

[a] Ting Wen, Ruixian Ding, Yannan Zhou, Yubing Si, Baocheng Yang Institute of Nanostructured Functional Materials, Huanghe Science and Technology College, Zhengzhou, Henan, 450006, China. E-mail: tingwen@infm.hhstu.edu.cn (T.W.); baochengyang@infm.hhstu.edu.cn (B.Y.)

[b] Ting Wen, Yannan Zhou, Yubing Si, Baocheng Yang Henan Provincial Key Laboratory of Nano-composite materials and Applications, Zhengzhou, Henan 450006, China.

[c] Yonggang Wang HPSynC, Geophysical Laboratory, Carnegie Institution of Washington, Argonne, IL 60439, USA. E-mail: yggwang@gmail.com (Y.W.)

Supporting information for this article is given via a link at the end of the document.

distinctive UC luminescence performances, e.g. multi-colour tunability and single-band UC outputs. Particularly, monoclinic ScOF was demonstrated to be a unique host for  $\text{RE}^{3+}$  UC generation, owing to the record-short Sc-Sc distance and the specific coordination environment of the doping sites with low-symmetry.<sup>13</sup> Nevertheless, none of these systems exhibits polymorphism or is phase-switchable, thus cannot be adopted for a structure-dependent study. Here, we report the fabrication of phase-pure erbium oxyfluoride with orthorhombic (O-ErOF) and rhombohedral (R-ErOF) structures using polytetrafluoroethylene (PTFE) as fluoridizer. The phase-temperature relationship of erbium oxyfluoride was characterized by powder X-ray diffraction at different reaction temperatures. An irreversible phase transition from O-ErOF to R-ErOF was disclosed by thermal analysis. Then, by means of photoluminescence spectroscopy,  $P-I$  curve and UC PL decay curves, we studied the UC luminescence characters of R-ErOF and O-ErOF and associated the UC properties with their crystal structures.

## Experimental Section

### Material syntheses

Powder samples of O-ErOF and R-ErOF were synthesized via a low-temperature fluorination route by adopting lanthanide oxides as raw materials and PTFE as the fluoridizer.<sup>14</sup> In a typical procedure, 0.383 g  $\text{Er}_2\text{O}_3$  (0.001 mol; >99.5%) and 0.1 g PTFE powder (0.002 mol  $\text{CF}_2$ ; >99%) were weighted and grounded together with ethanol for several minutes. The resulting fine powder was placed in an alumina crucible and sealed by an alumina cover. The sample was slowly heated to target temperature (300-1000 °C) with a heating rate of 5 °C/min. After holding at the reacting temperature for 5 hours, the furnace was allowed to cool down to room temperature naturally.

### Characterization

Powder X-ray diffraction (PXRD) data of all the samples were collected at room temperature (25 °C) on a Bruker D8 Advance diffractometer using a germanium monochromatic ( $\text{Cu K}\alpha$ ). The data in the  $2\theta$  range of 5-130° were collected in a step of 0.02° with the remaining time 1 s per step under the tube conditions 40 kV and 40 mV. The least-squares refinements of the cell parameters and atomic positions of the samples were performed adopting the known structures of YOF in the ICSD database as the initial models.<sup>15</sup>

The UC luminescence spectra were recorded on a modified Hitachi F-4500 spectrophotometer with a tunable 10 W 980 nm laser diode (Lasever Inc.) as the excitation source. The UC PL decay curves were measured using a FLS980 spectrophotometer equipped with a 150 W Xe lamp as the excitation source. All of the measurements were performed at room temperature. Thermogravimetric analysis (TG) and differential thermal analysis (DTA) measurements were conducted from room temperature up to 1000 °C using a thermobalance TA SDT Q600, with heating rate of 10 °C/min in air or  $\text{N}_2$  atmospheres, respectively. Raman spectra were

recorded on a Raman spectrometer with a 532.1 nm excitation laser.

## Results and Discussion

### Selective phase formation and the crystal structures

Previously, we demonstrated that a novel UC host, monoclinic scandium oxyfluoride, could be synthesized via a low-temperature fluorination route adopting PTFE as the fluoridizer.<sup>14</sup> It is highly expected that the facile method can be ported to the syntheses of other lanthanide oxyfluorides. Notably, in the case of erbium, it is found that one can not only fabricate phase-pure O-ErOF and R-ErOF using commercial erbium oxide as the raw material, but also realize phase selectivity by controlling the fluorination temperature and atmosphere in partially sealed alumina crucible.

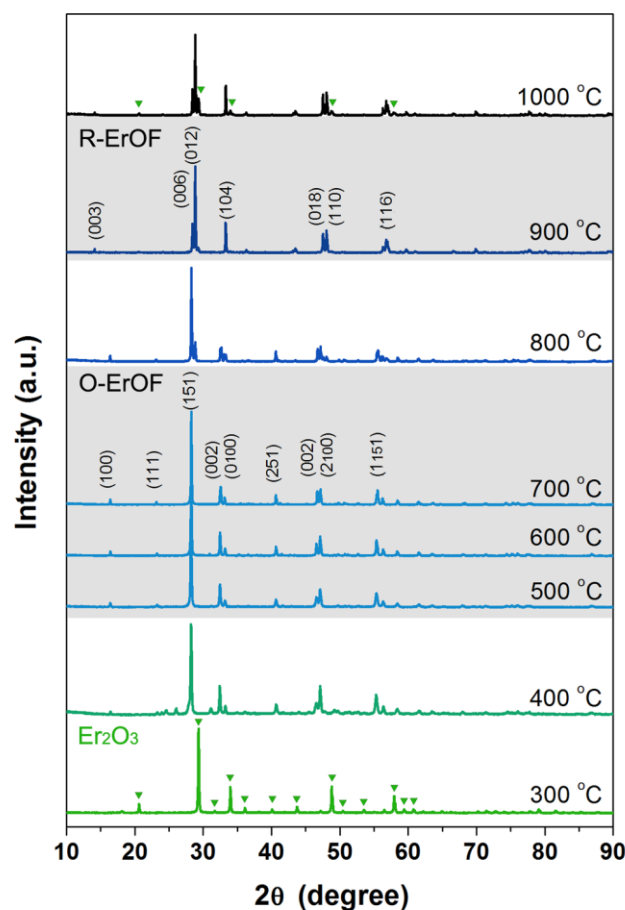


**Figure 1.** Powder X-ray diffraction patterns of as-synthesized powder samples with different sintering temperature in the range of 300-1000 °C. The green triangles indicate the diffraction peaks of  $\text{Er}_2\text{O}_3$ .

Fig. 1 shows the PXRD patterns of the products obtained with fixed  $\text{Er}_2\text{O}_3$ /PTFE ratio ( $\text{Er}/\text{F}=1:2$ ) and reaction period (4

h), but at different fluorination temperatures varying from 300 to 1000 °C. No reaction was observed below or at 300 °C since the diffraction peaks could be well assigned to the starting cubic  $\text{Er}_2\text{O}_3$ . At 400 °C, new peaks appeared in the products as a mixed phase and pure O-ErOF could be obtained in the temperature range of 500–700 °C. At 900 °C, another phase (R-ErOF) was obtained as a phase-pure product, while O- and R-ErOF coexisted around 800 °C. When the temperature reached as high as 1000 °C, cubic  $\text{Er}_2\text{O}_3$  reappeared due to the volatilization of PTFE and partial decomposition of R-ErOF. The details of the PXRD pattern in the range of 25–35° showing the phase evolution of O- and R-ErOF polymorphisms are provided in Fig. S1.

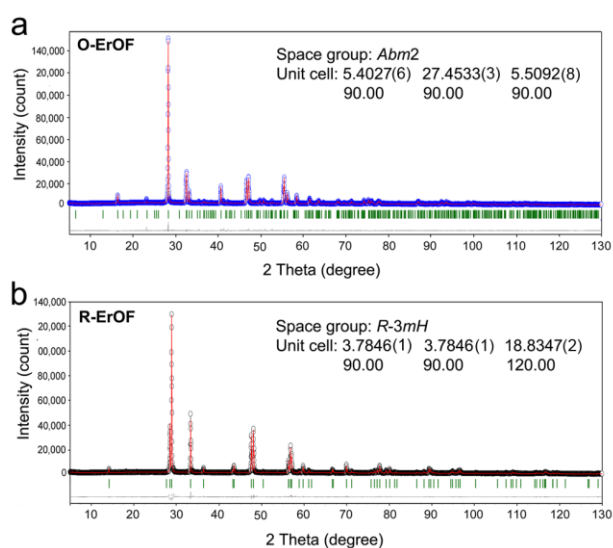


**Figure 2.** Rietveld refinement based on the powder X-ray diffraction data of: (a) O-ErOF annealed at 700 °C and (b) R-ErOF obtained at 900 °C.

The O-ErOF adopts the so-called “Vernier”-type structure, which is normally observed in lanthanide oxyfluorides for small lanthanides (Y, Lu, Yb) with general formula  $\text{RE}_n\text{O}_{n-1}\text{F}_{n+2}$ .<sup>16</sup> For erbium, only a  $n=3$  member ( $\text{Er}_3\text{O}_2\text{F}_5$ ) is available in the ICSD database, however, its XRD pattern does not match the as-obtained O-ErOF sample well (Fig. S2). Instead, a more elongated  $n=5$  orthorhombic unit cell can meet the as-obtained sample much better. LeBail fitting on the PXRD pattern of O-ErOF using orthorhombic space group *Abm2* gives cell parameters:  $a = 5.4027(6)$  Å,  $b = 5 \times 5.4907(3)$  Å and  $c = 5.5092(8)$  Å. A high  $n$  value Vernier-phase is reasonable for Er considering its similar ionic radius with Y and Lu. The formula  $\text{Er}_5\text{O}_4\text{F}_7$  was also roughly supported by the elemental measurement result. While, for the R-ErOF, LeBail fitting on the PXRD pattern yields a very good result with space group *R-3mH*,  $a = b = 3.7846(1)$  Å,  $c = 18.8347(2)$  Å. Rietveld refinement on the PXRD pattern of O-ErOF was performed using  $\text{Y}_5\text{O}_4\text{F}_7$  (ICSD#68949)<sup>17</sup> as the initial structure model. For brevity, the O/F distribution and disorder were treated by following those in  $\text{Y}_5\text{O}_4\text{F}_7$ . Rietveld refinement on R-ErOF was also performed using the known

structure of rhombohedral YOF (ICSD#14282)<sup>15</sup> as the initial model (as shown in Fig. 2b). The refinement plots are shown in Fig. 2. Detailed atomic positions and other structural parameters for O- and R-ErOF are listed in Table S1, S2, respectively.

The crystal structures of O- and R-ErOF are shown in Fig. 3. O-ErOF crystallizes in an elongated orthorhombic unit cell derived from fluorite-type structure, which has been proven as one of the best hosts for lanthanide UC generation. There are three crystallographic Er positions offered by the assorted array of  $\text{O}^{2-}$  and  $\text{F}^-$  ions surrounding the 8-fold coordinated  $\text{Er}^{3+}$  ions in the lattice, and they are arranged alternately along the  $b$ -axis. The partial ordering ( $8d$  site) and disorderly distribution of O/F ligands lead to the 5-fold elongation of the fluorite structure (i.e.,  $n$  in  $a \times nb \times c$ ). Despite their normal BVS values around +3 (Table S1), the three Er ions show distinct coordination environments, either in the number of O/F ligands or largely diverged bond lengths: Er1 in a  $C_1$  site coordinated with 4O and 4F, Er2 in a  $C_1$  site with 4F, 2O and 2O/F, and Er3 in a  $C_s$  site with 4O and 4O/F, respectively (Fig 3b). The diversity and low symmetry of the doping sites are considered in favour of  $f-f$  transitions. While for R-ErOF, the crystal structure is stoichiometric and highly ordered. The unique Er site is surrounded by 4O and 4F with trigonal symmetry along the  $c$ -axis. Compared with O-ErOF, such a highly-ordered host lattice is desirable for lanthanide UC with single-band outputs.

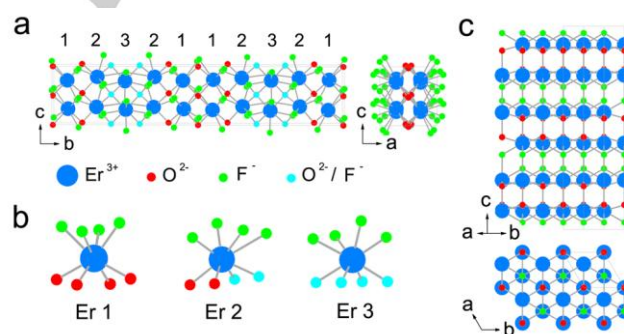


**Figure 3.** Crystal structures of O- and R-ErOF. (a) The orthorhombic structure of O-ErOF viewed along  $a$  and  $b$  axes. (b) The assorted array of  $\text{O}^{2-}$  and  $\text{F}^-$  ions offers three different types of  $\text{Er}^{3+}$  cation sites. Note that the  $\text{O}^{2-}$  and  $\text{F}^-$  anions located at  $8d$  sites shown as green balls are of disordered distribution; (c) The rhombohedral structure of R-ErOF presented as (110) and (001) sections.

### TG and DSC analysis

Besides the selective formation of O- and R-ErOF, it is also expected that one phase of ErOF can transfer to the other upon heating or cooling. TG and DSC analyses provide the thermal stability of O-ErOF and possible phase transition between O- and R-ErOF. As shown in Fig. 4, a sharp endothermic peak appears at 595.5 °C in the DSC curve for O-ErOF when subjected to high temperature in both air and nitrogen atmospheres. There is no obvious weight loss along with the endothermic process, which suggests a possible

structural phase transition to R-ErOF. Subsequently, the phase transition from O-ErOF to R-ErOF was confirmed by ex-situ sintering experiments, by which mass R-ErOF powders could be achieved from O-ErOF under heating above 600 °C for 3 h. The evolution of the PXRD patterns presenting the phase transition is provided in Fig. S3. An interesting question arising here is: why O-ErOF can form around 600 °C (Fig. 1) as well as transfer to R-ErOF at the same temperature? If one can realize that fluorination process is under a kinetically-controlled atmosphere, the different results under same temperature are not difficult to understand.

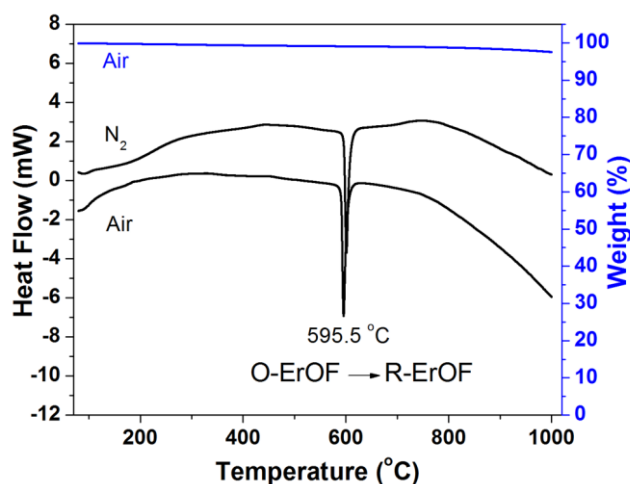


Figure 4. TG and DSC analysis of O-ErOF powder.

### UC PL properties of O- and R-ErOF

The as-prepared O- and R-ErOF with two distinct crystal structures provide a rare platform to study phase-dependent UC emission properties with lanthanide dopants. Besides the O-ErOF sample fabricated from PTFE fluorination route, two R-ErOF samples were adopted in the comparative studies: one was obtained from PTFE fluorination method (denoted as R-ErOF<sub>F</sub>), the other was obtained via phase transition from O-ErOF at 700 °C (denoted as R-ErOF<sub>PT</sub>). Fig. 5 shows the UC luminescence spectra of O-ErOF compared with those of R-ErOF<sub>F</sub> and R-ErOF<sub>PT</sub>. It is obvious that the UC emission outputs of both R-ErOF and R-ErOF<sub>PT</sub> are much stronger than that of O-ErOF<sub>F</sub> (200 and 30 times at 675 nm, respectively). This 675 nm red emission peak is attributed to the *f-f* transition  $^4F_{9/2} \rightarrow ^4I_{15/2}$ . Another minor green emission band near 545 nm can be assigned to the *f-f* transition  $^4S_{3/2} \rightarrow ^4I_{15/2}$ . Since particle size is another noticeable factor besides host structure determining the UC emission intensity, the impact from different sintering temperatures is evaluated by SEM images (Fig. S4). The particle size of R-ErOF<sub>F</sub> is much larger than that of O-ErOF. While for R-ErOF<sub>PT</sub>, phase transition from O-ErOF at relative low temperature (700 °C, the preparation temperature of O-ErOF) does not change the

particle size much (Fig. S5). Thus, the greatly enhanced UC PL emission from R-ErOF than that from O-ErOF is an intrinsic result due to their distinct crystal structure features.

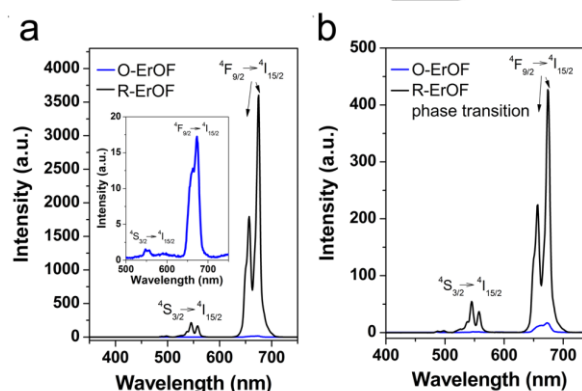
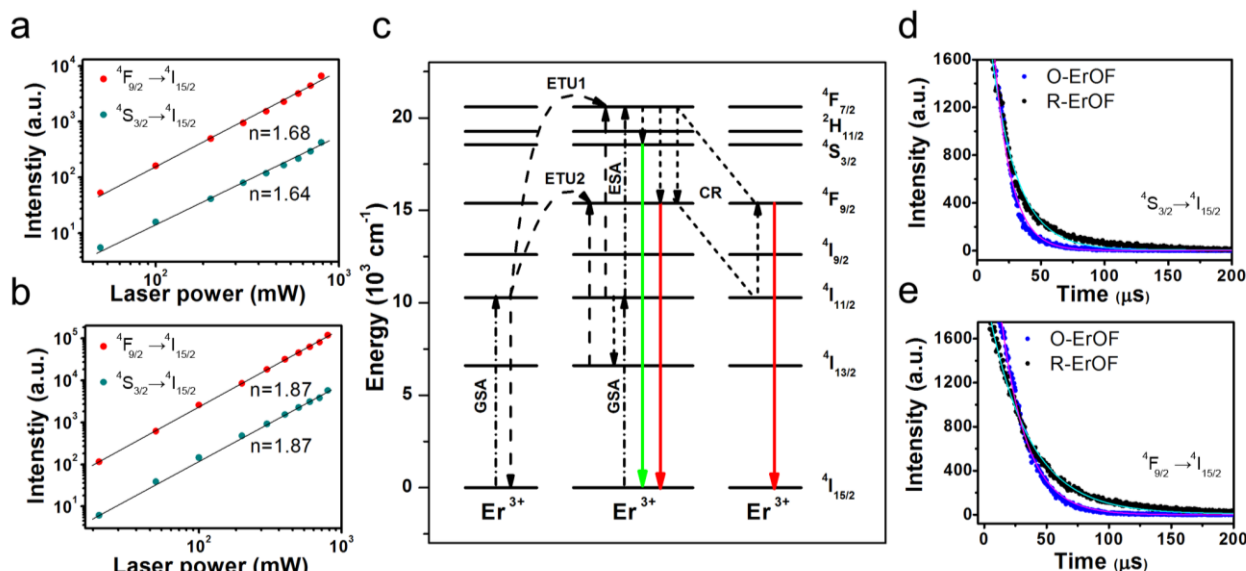


Figure 5. The UC emission spectra of the powder samples under 980 nm excitation ( $\sim 3 \text{ W cm}^{-2}$ ). (a) The UC emission spectra of O-ErOF and R-ErOF<sub>F</sub>; the inset shows the detail of the UC emission spectrum of O-ErOF in the range of 450-750 nm; (b) The UC emission spectra of O-ErOF and R-ErOF<sub>PT</sub>.

To gain further insight into the UC mechanisms of O- and R-ErOF, the UC intensities of green ( $^4S_{3/2} \rightarrow ^4I_{15/2}$ ) and red ( $^4F_{9/2} \rightarrow ^4I_{15/2}$ ) emissions were measured as a function of the pump power density  $P$  ( $P$ - $I$  curve) upon excitation at 980 nm. The  $P$ - $I$  measurements of O-ErOF and R-ErOF were plotted as double logarithmic scale curves in Fig. 6a and 6b, respectively. The slope values were determined to be 1.68 for O-ErOF and 1.87 for R-ErOF for the  $^4S_{3/2} \rightarrow ^4I_{15/2}$  transition, 1.64 for O-ErOF and 1.87 for R-ErOF for the  $^4F_{9/2} \rightarrow ^4I_{15/2}$  transition, respectively. It is known that the dependence of the UC emission intensity on the pump power density can be expressed as:  $I \propto P^n$ , where  $n$  is the number of pump photons corresponding to the slope in the double-logarithmic coordinate. Thus, the observed slopes above were indicative of two-photon pumping processes for the population of both  $^4S_{3/2}$  and  $^4F_{9/2}$ . The probable UC mechanism for O- and R-ErOF is schematically illustrated in Fig. 6c with the energy levels diagram of  $\text{Er}^{3+}$ . The two-photon pumping process comprises of a ground-state-absorption (GSA) and subsequent excited-state-absorption (ESA) process.  $^4F_{7/2}$  state can be also populated by non-radiative energy transfer process (ETU) from neighbouring  $\text{Er}^{3+}$  ion at the metastable level of  $^4I_{11/2}$  (ETU1) at the same time. With the non-radiative relaxation to the  $^4S_{3/2}$  and  $^4F_{9/2}$  levels, it results in corresponding green and red emissions. Another ETU process commonly occurs in high-doping UC materials should be indicated, that is, a photon at  $^4I_{11/2}$  level transits to the  $^4I_{13/2}$  state via a multi-phonon relaxation process and then is excited to  $^4F_{9/2}$  level through energy transfer from the  $^4I_{11/2}$  level of neighbouring  $\text{Er}^{3+}$  ion (ETU2). Besides, cross-relaxation (CR) process should be included into the energy migration process regarding the high  $\text{Er}^{3+}$  concentration.<sup>18</sup>



**Figure 6.** Log-log plots of the UC emission intensity versus the excitation power density under 980 nm excitation for: (a) O-ErOF and (b) R-ErOF samples. (c) Schematic energy level diagrams of the f-f transitions processes corresponding to the UC bands. Decay curves of the UC luminescence of O-ErOF and R-ErOF samples. UC decays of O-ErOF and R-ErOF from (d)  $^4S_{3/2} \rightarrow ^4I_{15/2}$  and (e)  $^4F_{9/2} \rightarrow ^4I_{15/2}$ .

Both ETU2 and CR are responsible for the strong red UC emission of  $Er^{3+}$  in both O- and R-ErOF.

UC PL decay behaviour is another useful evidence to identify the distinct UC processes in O- and R-ErOF (Fig. 6d, 6e). All the PL decay curves from  $^4S_{3/2}$  and  $^4F_{9/2}$  levels of O- and R-ErOF can be fitted well by using a single exponential function. The lifetime of the  $^4S_{3/2}$  state is 13.4  $\mu s$  for O-ErOF and 20.2  $\mu s$  for R-ErOF, and the lifetime of the  $^4F_{9/2}$  state is 20.8  $\mu s$  for O-ErOF and 32.7  $\mu s$  for R-ErOF, respectively. The lifetimes of  $^4F_{9/2}$  are much longer than those of  $^4S_{3/2}$  in both O- and R-ErOF, which indicates the significant contributions from the ETU2 and CR processes to  $^4F_{9/2}$  level. Besides, R-ErOF exhibits longer lifetimes in both  $^4S_{3/2}$  and  $^4F_{9/2}$  states compared with those of O-ErOF, probably owing to the distinct features of their crystal structures.

In lanthanide UC materials, the activator ion is always controlled at a relatively low concentration to avoid unfavourable cross-relaxation process among the RE ions. It is worth noting that ErOF can be considered as a highly self-doped host material, where cross-relaxation may lead to serious quenching of the excited state.<sup>2</sup> However, there are still several reports of highly doped RE UC materials in which concentration quenching is supposed that can be suppressed geometrically at sub-lattice scale.<sup>19</sup> The basic principle is that, the energy transfer probability highly depends on the migration distances between adjacent active ions located on the sub-lattice.<sup>3</sup> This may also be applied to explain the UC intensity difference between O- and R-ErOF. The probability of energy transfer between two adjacent  $Er^{3+}$  follows the relationship:  $P = C_{Er-Er} \exp(-2R/L)$ , where  $R$  is the distance between the energy donor-acceptor pair,  $C_{Er-Er}$  is the Er-Er interaction constant, and  $L$  is the effective Bohr radius. The closer is the Er-Er distance, the higher is the probability of energy transfer between them.

Fig. 7 shows the quasi-layered structures for O- and R-ErOF and the arrangement of Er atoms in both phases. In O-ErOF, the intra-layer Er-Er distance is mainly distributed in 3.56-3.73  $\text{\AA}$  and the inter-layer Er-Er distance varies from 4.13 to 4.16  $\text{\AA}$ . While, in R-ErOF, there are only two intra-layer Er-Er distances of 3.58 and 3.78  $\text{\AA}$ , and an inter-layer distance of 4.08  $\text{\AA}$ . The  $Er^{3+}$  ions in R-ErOF arrange in a much more ordered manner and each  $Er^{3+}$  ion is compassed regularly by three closest  $Er^{3+}$  ions. Contrastively, all the  $Er^{3+}$  ions in O-ErOF are surrounded randomly by four to six closest  $Er^{3+}$  ions in a narrow range of 3.56-3.64  $\text{\AA}$ . More energy migration pathways in O-ErOF may lead to more cross-relaxation for energy loss. Moreover, the energy migration to the crystal defects is also regarded as a possible reason for the concentration quenching in high doping

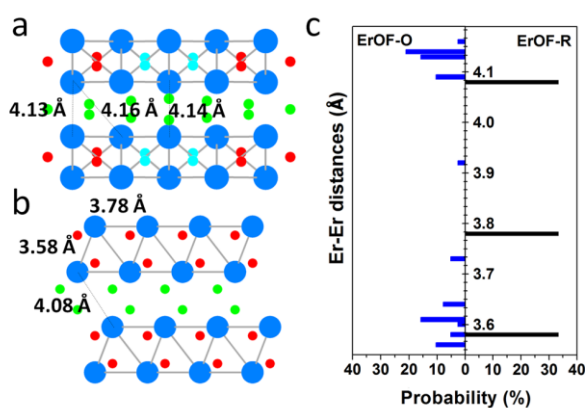


**Figure 7.** Schematic representation of Er-Er distances in the layered sub-lattice: (a) O-ErOF and (b) R-ErOF. (c) The compare of Er-Er distances distribution between O-ErOF and R-ErOF.

crystalline materials.<sup>20</sup> Fig. S6 shows the Raman spectroscopy of O- and R-ErOF samples. Several sharp Raman peaks in the 200-1000 cm<sup>-1</sup> region are observed for R- ErOF. Comparatively, for O-ErOF, the Raman bands are broad and with low intensity, indicating the highly disordered structure features and the existence of structure defects in the host lattice.<sup>21</sup> However, the detailed local structure study need further characterizations such as pair-distribution-function and extended X-ray absorption fine structure spectrometer.

## Conclusions

In summary, we reported a facile fluorination route to orthorhombic and rhombohedral erbium oxyfluorides. Both phases can be selectively achieved with high purity by simply controlling the sintering temperature. O-ErOF can also transform to R-ErOF via a structural phase transition upon heating around 600 °C. R-ErOF shows stronger UC emission than that of O-ErOF. Comprehensive and comparative studies on the UC PL behaviours of O- and R-ErOF were performed by using PL, *P-I* and UC decay curves. The structure features of O- and R-ErOF at sub-lattice scale are supposed responsible for the distinct UC PL outputs. Our demonstration offers a new perspective to understand the impact of crystal structure for UC PL properties.

## Acknowledgements

This work was supported by National Natural Science Foundation of China 51602119, Natural Science Foundation of Education Department of Henan 17A150014 and Key Project of Science and Technology of Zhengzhou 153PKJGG139.

**Keywords:** Selective synthesis, Up-conversion, Phase transition, Oxyfluoride

- [1] a) J. Büünzli and C. Piguet, *Chem. Soc. Rev.*, **2005**, *34*, 1048-1077. b) F. Wang and X. Liu, *Chem. Soc. Rev.*, **2009**, *38*, 976-989. c) M. Haase and H. Schäfer, *Angew. Chem., Int. Ed.*, **2011**, *50*, 5808-5829. d) L. Wang, P. Li and Y. Li, *Adv. Mater.*, **2007**, *19*, 3304-3307. e) C. Jiang, F. Wang, N. Wu and X. Liu, *Adv. Mater.*, **2008**, *20*, 4826-4829. f) F. Wang and X. Liu, *J. Am. Chem. Soc.*, **2008**, *130*, 5642-5643. g) S. Eliseeva and J. Büünzli, *Chem. Soc. Rev.*, **2010**, *39*, 189-227. h) Y. Park, J. Kim, K. Lee, K. Jeon, H. Na, J. Yu, H. M. Kim, N. Lee, S. Choi, S. Baik, H. Kim, S. Park, B. Park, Y. Kim, S. Lee, S. Yoon, I. Song, W. Moon, Y. Suh and T. Hyeon, *Adv. Mater.*, **2009**, *21*, 4467-4471. i) D. Chatterjee, M. Gnanasamandhan and Y. Zhang, *Small*, **2010**, *6*, 2781-2795. j) L. Wang and Y. Li, *Chem. Commun.*, **2006**, 2557-2559. k) Z. Gu, L. Yan, G. Tian, S. Li, Z. Chai and Y. Zhao, *Adv. Mater.*, **2013**, *25*, 3758-3779.
- [2] F. Wang and X. Liu, *Chem. Soc. Rev.*, **2009**, *38*, 976-989.
- [3] a) J. Wang, R. Deng, M. MacDonald, B. Chen, J. Yuan, F. Wang, D. Chi, T. Andy Hor, P. Zhang, G. Liu, Y. Han and X. Liu, *Nat. Mater.*, **2013**, *13*, 157-162. b) Z. Xia, C. Ma, M. S. Molokeev, Q. Liu, K. Rickert and K. R. Poeppelmeier, *J. Am. Chem. Soc.*, **2015**, *137*, 12494-12497. c) Z. Xia, G. Liu, J. Wen, Z. Mei, M. Balasubramanian, M. S. Molokeev, L. Peng, L. Gu, D. J. Miller, Q. Liu and K. R. Poeppelmeier, *J. Am. Chem. Soc.*, **2016**, *138*, 1158-1161. d) M. Chen, Z. Xia, M. S. Molokeev, T. Wang and Q. Liu, *Chem. Mater.*, **2017**, *29*, 1430-1438.
- [4] S. Heer, K. Kömpe, H. Güdel and M. Haase, *Adv. Mater.*, **2004**, *16*, 2102-2105.
- [5] a) D. Klier and M. Kumke, *J. Mater. Chem. C*, **2015**, *3*, 11228-11238. b) H. Mai, Y. Zhang, L. Sun and C. Yan, *J. Phys. Chem. C*, **2007**, *111*, 13730-13739. c) K. Krämer, D. Biner, G. Frei, H. Güdel, M. Hehlen and S. Lüthi, *Chem. Mater.*, **2004**, *16*, 1244-1251.
- [6] F. Wang, Y. Han, C. Lim, Y. Lu, J. Wang, J. Xu, H. Chen, C. Zhang, M. Hong and X. Liu, *Nature*, **2010**, *463*, 1061-1065.
- [7] a) X. Sun, Y. W. Zhang, Y. Du, Z. G. Yan, R. Si, L. You and C. Yan, *Chem. Eur. J.*, **2006**, *13*, 2320-2332. b) T. Grzyb and S. Lis, *Inorg. Chem.*, **2011**, *50*, 8112-8120. c) L. Armelao, G. Bottaro, L. Bovo, C. Maccato, M. Pascolini, C. Sada, E. Soini and E. Tondello, *J. Phys. Chem. C*, **2009**, *113*, 14429-14434. d) Y. Du, Y. Zhang, L. Sun and C. Yan, *J. Phys. Chem. C*, **2008**, *112*, 405-415. e) M. Shang, G. Li, X. Kang, D. Yang, D. Geng, C. Peng, Z. Cheng, H. Lian and J. Lin, *Dalton Trans.*, **2012**, *41*, 5571-5580. f) Y. Du, Y. Zhang, Z. Yan, L. Sun and C. Yan, *J. Am. Chem. Soc.*, **2009**, *131*, 16364-16365. g) M. Shang, D. Geng, X. Kang, D. Yang, Y. Zhang and J. Lin, *Inorg. Chem.*, **2012**, *51*, 11106-11116. h) Y. Zhang, X. Li, X. Kang, Z. Hou and J. Lin, *Phys. Chem. Chem. Phys.*, **2014**, *16*, 10779-10787. i) K. Zheng, Y. Liu, Z. Liu, Z. Chen and W. Qin, *Dalton Trans.*, **2013**, *42*, 5159-5166. j) T. Grzyb and A. Tyminski, *J. Alloys Compd.*, **2016**, *660*, 235-243.
- [8] T. Passuello, F. Piccinelli, M. Trevisani, M. Giarola, G. Mariotto, L. Marciniak, D. Hreniak, M. Guzik, M. Fasoli, A. Vedda, V. Jary, M. Nikl, V. Causin, M. Bettinellia and A. Speghini, *J. Mater. Chem.*, **2012**, *22*, 10639-10649.
- [9] a) F. Wang, Y. Han, C. Lim, Y. Lu, J. Wang, J. Xu, H. Chen, C. Zhang, M. Hong and X. Liu, *Nature*, **2010**, *463*, 1061-1065. b) G. Wang, Q. Peng and Y. Li, *J. Am. Chem. Soc.*, **2009**, *131*, 14200-14201. c) D. Bevan, J. Mohyla, B. Hoskins and R. Steen, *Eur. J. Solid State Inorg. Chem.*, **1990**, *27*, 451-465.
- [10] a) T. Passuello, F. Piccinelli, M. Trevisani, M. Giarola, G. Mariotto, L. Marciniak, D. Hreniak, M. Guzik, M. Fasoli, A. Vedda, V. Jary, M. Nikl, V. Causin, M. Bettinellia and A. Speghini, *J. Mater. Chem.*, **2012**, *22*, 10639-10649. b) B. Hyde, A. Bagshaw, S. Anderson and M. O'Keefe, *Annu. Rev. Mater. Sci.*, **1974**, *4*, 43-91.
- [11] O. Janka and T. Schleid, *Eur. J. Inorg. Chem.* **2009**, 357-362
- [12] a) T. Wen, W. Luo, Y. Wang, M. Zhang, Y. Guo, J. Yuan, J. Ju, F. Liao and B. Yang, *J. Mater. Chem. C*, **2013**, *1*, 1995-2001. b) W. Luo, Y. Wang, Y. Chen, T. Wen, M. Liu, Y. Wang, F. Liao and J. Lin, *J. Mater. Chem. C*, **2013**, *1*, 5711-5717. c) Y. Wang, T. Wen, H. Zhang, J. Sun, M. Zhang, Y. Guo, W. Luo, M. Xia, Y. Wang and B. Yang, *J. Phys. Chem. C*, **2014**, *118*, 10314-10320.
- [13] T. Wen, Y. Zhou, Y. Guo, C. Zhao, B. Yang and Y. Wang, *J. Mater. Chem. C*, **2016**, *4*, 684-690.
- [14] S. Dutton, D. Hirai and R. Cava, *Mater. Res. Bull.*, **2012**, *47*, 714-718.
- [15] A. W. Mann, D. J. M. Bevan, *Acta Cryst. B*, **1982**, *24*, 1183-1190.
- [16] a) D. Bevan, J. Mohyla, B. Hoskins and R. Steen, *Eur. J. Solid State Inorg. Chem.*, **1990**, *27*, 451-465. c) Y. Wang, T. Wen, H. Zhang, J. Sun, M. Zhang, Y. Guo, W. Luo, M. Xia, Y. Wang and B. Yang, *J. Phys. Chem. C*, **2014**, *118*, 10314-10320. c) T. Wen, Y. Zhou, Y. Guo, C. Zhao, B. Yang and Y. Wang, *J. Mater. Chem. C*, **2016**, *4*, 684-690.
- [17] D. Bevan, J. Mohyla, B. Hoskins and R. Steen, *Eur. J. Solid State Inorg. Chem.*, **1990**, *27*, 451-465.
- [18] a) C. Mi, J. Wu, Y. Yang, B. Han and J. Wei, *Sci. Rep.*, **2016**, *6*, 22545-22556. b) W. Wei, Y. Zhang, R. Chen, J. Goggi, N. Ren, L.

- Huang, K. Bhakoo, H. Sun and T. Tan, *Chem. Mater.*, **2014**, *26*, 5183-5186.
- [19] a) J. Wang, R. Deng, M. MacDonald, B. Chen, J. Yuan, F. Wang, D. Chi, T. Andy Hor, P. Zhang, G. Liu, Y. Han and X. Liu, *Nat. Mater.*, **2013**, *13*, 157-162. b) T. Wen, Y. Zhou, Y. Guo, C. Zhao, B. Yang and Y. Wang, *J. Mater. Chem. C*, **2016**, *4*, 684-690.
- [20] a) J. Stouwdam and V. Veggel, *Nano. Lett.*, **2002**, *2*, 733-737. b) N. Johnson, S. He, S. Diao, E. Chan, H. Dai and A. Almutairi, *J. Am. Chem. Soc.*, **2017**, *139*, 3275-3282.
- [21] a) D. Argyriou, H. Bordallo, B. Campbell, A. Cheetham, D. Cox, J. Gardner, K. Hanif, A. Santos and G. Strouse, *Phys. Rev. B*, **2000**, *22*, 15269-15276. b) S. Loidant, G. Lucazeau and T. Le-Bihan, *J. Phys. Chem. Solids*, **2002**, *63*, 1983-1992.

WILEY-VCH

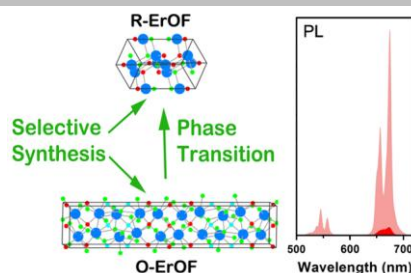
Accepted Manuscript

**Entry for the Table of Contents** (Please choose one layout)

Layout 1:

## FULL PAPER

Phase-pure orthorhombic and rhombohedral erbium oxyfluorides (O-ErOF and R-ErOF) were obtained selectively. An irreversible phase transition was observed from O-ErOF to R-ErOF around 700 °C and the anomalous upconversion behaviour of the two polymorphisms was associated with their distinct structure features.

**Key Topic\* Phase-selective synthesis**

Ting Wen,\* Ruixian Ding, Yannan Zhou, Yubing Si, Baocheng Yang\* and Yonggang Wang\*

Page No. – Page No.

**Polymorphism of Erbium Oxyfluoride: Selective Synthesis, Crystal Structure and Phase-Dependent Upconversion Luminescence**

\*one or two words that highlight the emphasis of the paper or the field of the study